



This is a repository copy of *Engineering semiconductor quantum dots for selectivity switch on high-performance heterogeneous coupling photosynthesis*.

White Rose Research Online URL for this paper:

<https://eprints.whiterose.ac.uk/192434/>

Version: Accepted Version

---

**Article:**

Qi, M.-Y., Conte, M. [orcid.org/0000-0002-1399-0344](https://orcid.org/0000-0002-1399-0344), Tang, Z.-R. et al. (1 more author) (2022) Engineering semiconductor quantum dots for selectivity switch on high-performance heterogeneous coupling photosynthesis. *ACS Nano*, 16 (10). pp. 17444-17453. ISSN 1936-0851

<https://doi.org/10.1021/acsnano.2c08652>

---

This document is the Accepted Manuscript version of a Published Work that appeared in final form in *ACS Nano*, copyright © American Chemical Society after peer review and technical editing by the publisher. To access the final edited and published work see <https://doi.org/10.1021/acsnano.2c08652>

**Reuse**

Items deposited in White Rose Research Online are protected by copyright, with all rights reserved unless indicated otherwise. They may be downloaded and/or printed for private study, or other acts as permitted by national copyright laws. The publisher or other rights holders may allow further reproduction and re-use of the full text version. This is indicated by the licence information on the White Rose Research Online record for the item.

**Takedown**

If you consider content in White Rose Research Online to be in breach of UK law, please notify us by emailing [eprints@whiterose.ac.uk](mailto:eprints@whiterose.ac.uk) including the URL of the record and the reason for the withdrawal request.



[eprints@whiterose.ac.uk](mailto:eprints@whiterose.ac.uk)  
<https://eprints.whiterose.ac.uk/>

1  
2  
3  
4  
5  
6  
7 **Engineering Semiconductor Quantum Dots for**  
8  
9  
10 **Selectivity Switch on High-Performance**  
11  
12  
13 **Heterogeneous Coupling Photosynthesis**  
14  
15

16  
17 *Ming-Yu Qi,<sup>1</sup> Marco Conte,<sup>2</sup> Zi-Rong Tang,<sup>1</sup> and Yi-Jun Xu<sup>\*1</sup>*  
18

19  
20 <sup>1</sup> College of Chemistry, State Key Laboratory of Photocatalysis on Energy and Environment,  
21 Fuzhou University, Fuzhou, 350116, China.  
22

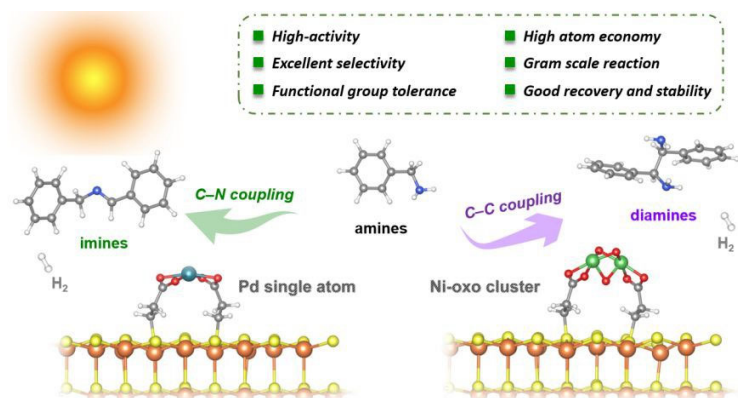
23  
24 <sup>2</sup> Department of Chemistry, University of Sheffield, Sheffield, S3 7HF, UK.  
25  
26  
27  
28  
29  
30  
31  
32  
33  
34  
35  
36  
37  
38  
39  
40  
41  
42  
43  
44  
45  
46  
47  
48  
49  
50  
51  
52  
53  
54  
55  
56  
57  
58  
59  
60

**Abstract**

Semiconductor-based photoredox catalysis brings an innovative strategy for sustainable organic transformation, *e.g.*, C–C/C–X bond formation, *via* radical coupling under mild conditions. However, since semiconductors interact with photogenerated radicals unselectively, the precise control of selectivity for such organic synthesis by steering radical conversion is extremely challenging. Here, by the judicious design of structurally well-defined and atomically dispersed cocatalyst over semiconductor quantum dots, we demonstrate the precise selectivity switch on high-performance selective heterogeneous coupling photosynthesis of C–C bond or C–N bond along with hydrogen production over the Ni-oxo cluster and single Pd atom-decorated CdS quantum dots crafted onto the SiO<sub>2</sub> support. Mechanistic studies unveil that the Ph( $\bullet$ CH)NH<sub>2</sub> and PhCH<sub>2</sub>NH<sub>2</sub><sup>•+</sup> act as dominant radical intermediates for such divergent organic synthesis of C–C coupled vicinal diamines and C–N coupled imines, as respectively enabled by Ni-oxo clusters assisted radical-radical coupling and single Pd atom assisted radical addition-elimination. This work overcomes the pervasive difficulties of selectivity regulation in semiconductor-based photochemical synthesis, highlighting a vista of utilizing atomically dispersed cocatalysts as active sites to maneuver unselective radical conversion by engineering quantum dots toward selective heterogeneous photosynthesis.

**KEYWORDS:** artificial photosynthesis, covalent-assembly, semiconductor quantum dots, atomically dispersed cocatalysts, C–X bond formation

## TOC GRAPHICS



1  
2  
3 Organic transformations involving C–C/C–X bond (X = N, O, S) formation are of  
4 paramount significance in the synthesis of pharmaceuticals and fine chemicals.<sup>1–3</sup> Over the past  
5 decade, photoredox catalysis has been recognized as a powerful technique for such organic  
6 synthesis, most prominently with the generation of highly reactive intermediates, *i.e.*, carbon-  
7 and heteroatom-centered radicals as an enabling platform.<sup>4–7</sup> Traditionally, these radicals are  
8 accessed *via* well-known single electron transfer (SET) between organic substrates and the triplet  
9 excited state of  $d^6$  transition-metal complexes (especially [Ru] and [Ir]) generated through  
10 visible-light-induced metal to ligand charge transfer (MLCT).<sup>4–5, 8</sup> Due to the intrinsic advantages  
11 of defined coordination geometry, active center and ligands, these transition-metal complexes as  
12 homogeneous photocatalysts can be modified rationally to a given selective organic synthesis  
13 such as C–X bond formation.<sup>5, 9</sup> However, most of the molecular transition-metal complexes for  
14 triplet-initiated reactions are not stable,<sup>10</sup> and these homogeneous catalytic systems are often  
15 plagued by the effective product/catalyst separation and catalyst recycling.<sup>9–11</sup>  
16  
17  
18  
19  
20  
21  
22  
23  
24  
25  
26

27 Semiconductor-based heterogeneous photocatalysis has emerged as an alternative to initiate  
28 radical coupling reactions for C–C/C–X bond synthesis owing to its high efficiency and  
29 convenience in the generation of various high-reactive radical species *via* charge transfer  
30 between organic molecules and semiconductors under mild conditions.<sup>12</sup> However, since  
31 semiconductors interact with photogenerated radicals unselectively,<sup>13</sup> the precise control of  
32 selectivity by steering radical conversion is extremely challenging for C–C/C–X bond synthesis  
33 on the surface of semiconductors. As a bridge between homo- and heterogeneous catalysis,  
34 atomically dispersed catalysts render the merits of homogeneous catalysts, including the well-  
35 defined active sites and the tunable interactions with ligands, and inherit the high durability and  
36 excellent recoverability as heterogeneous catalysts.<sup>14–15</sup> In particular, the uniform active sites,  
37 featuring unsaturated coordination sites and characteristic electronic structures, are expected to  
38 unlock exclusively high activity and selectivity.<sup>14–17</sup> In this regard, the rational design of  
39 semiconductor-based photocatalysts with the body of heterogeneous catalysts and the soul of  
40 homogeneous catalysts by incorporating atomically dispersed metal guest with the host  
41 semiconductor, would be a powerful but yet-to-be-realised strategy toward real-life and scalable  
42 solar-driven photoredox organic synthesis.  
43  
44  
45  
46  
47  
48  
49  
50  
51  
52  
53  
54  
55  
56  
57  
58  
59  
60

1  
2  
3  
4 Herein, taking amines, the most versatile building blocks for the synthesis of N-containing  
5 compounds, as proof-of-concept model molecules,<sup>18-20</sup> we report the judicious design of  
6 structurally well-defined Ni or Pd-decorated CdS quantum dots (QDs) crafted onto spherical  
7 SiO<sub>2</sub> (M-CdS/SiO<sub>2</sub>, M=Ni or Pd) as the robust, heterogeneous catalyst for the high-performance  
8 photochemical coupling of amines into tunable C–C coupled vicinal diamines or C–N coupled  
9 imines concomitantly with hydrogen (H<sub>2</sub>) production at ambient conditions. High-reactive C-  
10 centered radicals (Ph(•CH)NH<sub>2</sub>) are generated *via* the electron transfer followed by proton  
11 transfer between benzylamine molecules and photoexcited CdS QDs. Atomically dispersed Ni or  
12 Pd species act as active sites to steer Ph(•CH)NH<sub>2</sub> radical conversion pathway for precisely  
13 controlling the photochemical selectivity switch between C–C and C–N bond formation reaction  
14 along with enhanced activity, *i.e.*, direct C–C coupling of Ph(•CH)NH<sub>2</sub> for vicinal diamines  
15 synthesis by Ni-oxo clusters-assisted catalysis and C–N coupling of aldimine intermediate  
16 (Ph(CH)NH, generated from the dehydrogenation of Ph(•CH)NH<sub>2</sub>) for imines synthesis by single  
17 Pd atoms-assisted catalysis. The use of SiO<sub>2</sub> support and robust covalent-assembly strategy  
18 significantly improves the anti-photocorrosion and recycling capability of M-CdS QDs. The  
19 successful gram-scale synthesis and sun-light irradiation experiment further showcase the  
20 significant potential of the present artificial photosynthesis system for real scale-up applications.  
21  
22  
23  
24  
25  
26  
27  
28  
29  
30  
31  
32  
33

## 34 Results and Discussion

### 35 Preparation and characterization of the M-CdS/SiO<sub>2</sub>

36  
37 To overcome the drawbacks of weak interfacial interaction, poor anti-leaching capability  
38 and low-loading net content of photoactive particles in previous electrostatic self-assembly  
39 approach,<sup>21-23</sup> we herein turn to adopt a robust covalent-assembly approach (**Figure 1a** and **S1**)  
40 to achieve efficient interfacial binding and improve the loading amount of photoactive CdS QDs  
41 onto SiO<sub>2</sub> support before crafting atomically dispersed metal cocatalysts. This covalent-based  
42 interfacial engineering approach is inspired from the application of 1-(3-  
43 (dimethylamino)propyl)-3-ethylcarbodiimide hydrochloride (EDC)/N-hydroxysuccinimide  
44 (NHS) cross-linking reaction for the formation of amide bonds in the assemble/modification of  
45 proteins.<sup>24-27</sup> In our designed synthesis methodology, the SiO<sub>2</sub> supports are firstly modified by  
46 branched poly-ethylenimine (BPEI) for grafting with –NH<sub>2</sub> groups;<sup>21, 23</sup> whereas CdS QDs are  
47 prepared using 3-mercaptopropionic acid (MPA) as capping molecule,<sup>23</sup> which serves as a  
48 stabilizer to disperse QDs and provides –COOH groups for grafting with SiO<sub>2</sub>. After activation  
49  
50  
51  
52  
53  
54  
55  
56  
57  
58  
59  
60

1  
2  
3 of the  $-\text{COOH}$  groups in CdS QDs by EDC/NHS, amidation reaction can occur smoothly to  
4 form a covalent amide bond, thereby robustly linking MPA-CdS QDs and BPEI-SiO<sub>2</sub> support.  
5 Upon grafting MPA-CdS QDs onto BPEI-SiO<sub>2</sub> support, a binding energy located at 287.1 eV,  
6 corresponding to the newly formed amide bond ( $-\text{CON}-$ ), is observed in the C 1s X-ray  
7 photoelectron spectroscopy (XPS) spectrum of CdS-SiO<sub>2</sub> (**Figure S2**).<sup>28-29</sup> This is also detected  
8 by the N 1s and O 1s XPS spectra, in which the featured peaks appeared at 397.2 eV of N 1s  
9 region and 530.1 eV of O 1s region are both attributed to  $-\text{CON}-$  bond.<sup>29-30</sup> The formation of an  
10 amide bond was further confirmed by Fourier-transform infrared spectroscopy (**Figure S3**). It is  
11 evident that utilizing such EDC/NHS covalent-assembly approach is able to realize the effective  
12 chemical grafting of CdS QDs onto SiO<sub>2</sub> supports. Consequently, as compared to electrostatic  
13 self-assembly approach, this robust covalent-assembly approach not only achieves a high QDs  
14 loading of approximately 15 wt% onto SiO<sub>2</sub> spheres (see **Figure S4-6** for crystal structures,  
15 morphologies, and optical absorption properties), but also endows CdS/SiO<sub>2</sub> with ultra-low  
16 element leakage after the photochemical reaction as will be discussed below.  
17  
18

19  
20  
21  
22  
23  
24  
25  
26  
27  
28 Upon achieving the robust binding and high loading of CdS QDs onto SiO<sub>2</sub> supports by  
29 such covalent-assembly approach, we further decorated the well-fabricated CdS/SiO<sub>2</sub> with  
30 atomically dispersed metal (single-atom or cluster) cocatalysts through a facile *in-situ*  
31 photodeposition strategy (**Figure 1a**). In our approach, CdS/SiO<sub>2</sub> contains residual dangling  $-\text{COOH}$   
32 groups, which can serve as a rigid ligand to adsorb and anchor Pd<sup>2+</sup> (or Ni<sup>2+</sup>) cations.  
33 Photodeposition of Pd (or Ni) species was carried out using PdCl<sub>2</sub> (NiCl<sub>2</sub>·6H<sub>2</sub>O for Ni) as a  
34 precursor in aqueous solution, which was irradiated with a xenon lamp for 0.5 h. No formation of  
35 Pd or Ni-derived nanoparticles is observed in high-resolution transmission electron microscopy  
36 (TEM) images (**Figure S7** and **S8**) of the obtained M-CdS/SiO<sub>2</sub> (M=Ni or Pd). Elemental  
37 mapping results of the individual M-CdS/SiO<sub>2</sub> sphere (**Figure S7e** and **S8e**) reveal that the Pd or  
38 Ni element is evenly distributed in the surface of CdS/SiO<sub>2</sub>, and the aberration-corrected high-  
39 angle annular dark-field scanning TEM (HAADF-STEM) images certify that the Pd or Ni  
40 species is atomically dispersed on CdS/SiO<sub>2</sub> (**Figure S9**).  
41  
42  
43  
44  
45  
46  
47  
48  
49  
50  
51  
52  
53  
54  
55  
56  
57  
58  
59  
60

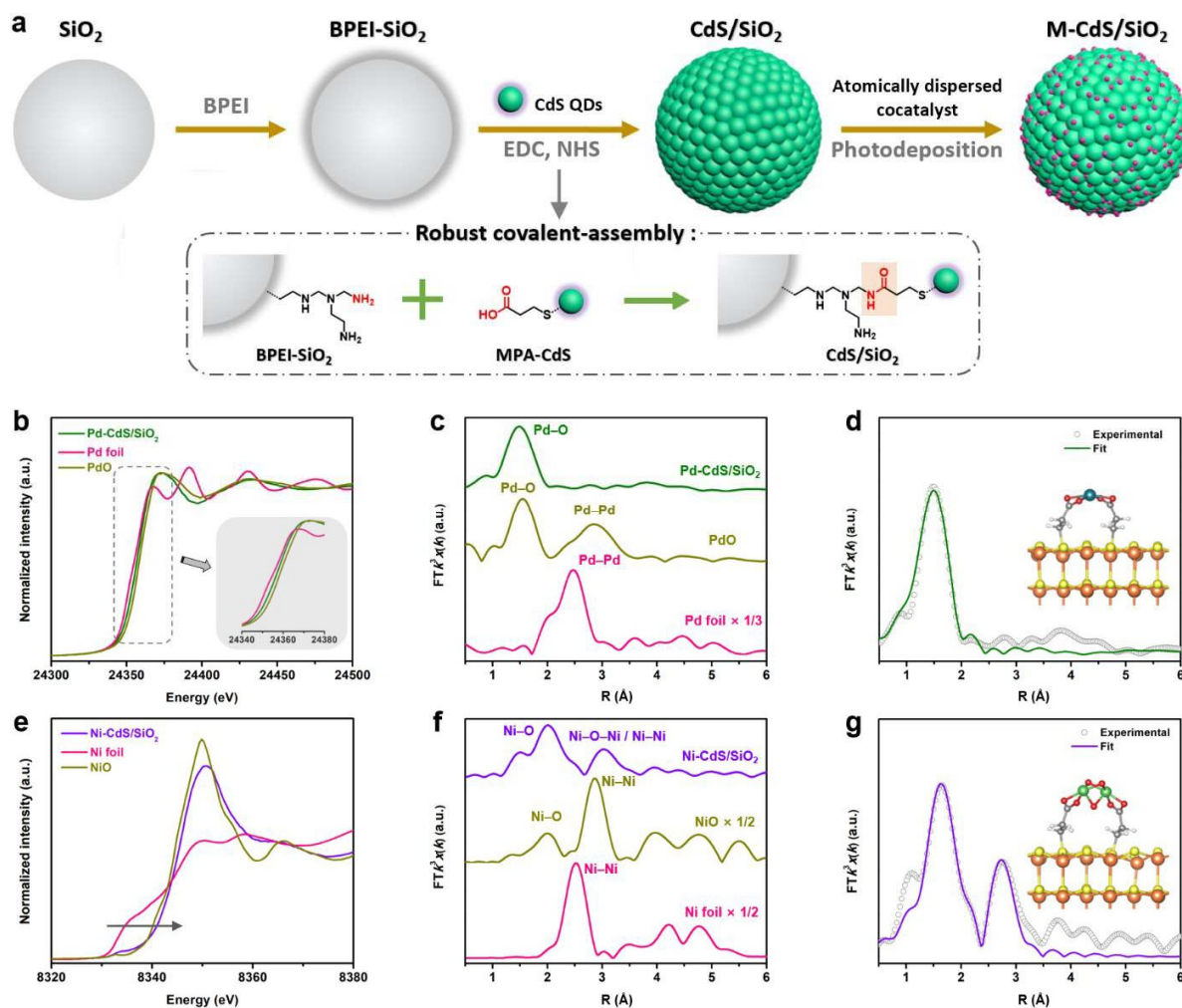


**Figure 1.** (a) Synthesis procedure for the M-CdS/SiO<sub>2</sub> composite (M=Ni or Pd). (b) Normalized Pd K-edge XANES spectra of Pd-CdS/SiO<sub>2</sub> in reference to Pd foil and PdO. (c) FT-EXAFS spectra of Pd-CdS/SiO<sub>2</sub> in reference to Pd foil and PdO. (d) The corresponding EXAFS fitting curves for Pd-CdS/SiO<sub>2</sub>. (e) Normalized Ni K-edge XANES spectra of Ni-CdS/SiO<sub>2</sub> in reference to Ni foil and NiO. (f) FT-EXAFS spectra of Ni-CdS/SiO<sub>2</sub> in reference to Ni foil and NiO. (g) The corresponding EXAFS fitting curves for Ni-CdS/SiO<sub>2</sub>. Insets in **Figure 1d** and **g** are the structures of Pd-CdS/SiO<sub>2</sub> and Ni-CdS/SiO<sub>2</sub> optimized by first principle DFT calculations. Atoms in cyan, green, red, brown, yellow, grey and white represent Pd, Ni, O, Cd, S, C and H respectively.

To further investigate the local coordination environment of atomically dispersed Pd or Ni species, X-ray absorption spectroscopy (XAS) measurements were carried out. **Figure 1b** shows

1  
2  
3 the Pd K-edge X-ray absorption near-edge structure (XANES) spectrum of Pd-CdS/SiO<sub>2</sub>, along  
4 with Pd foil and PdO as references. Evidently, the threshold energy ( $E_0$ ) of the Pd K-edge for Pd-  
5 CdS/SiO<sub>2</sub> is between that of PdO and Pd foil, and the XANES white line peak of Pd-CdS/SiO<sub>2</sub> is  
6 very close to that of PdO, demonstrating that the electronic state of Pd in Pd-CdS/SiO<sub>2</sub>  
7 approximates to +2.<sup>31</sup> Processed through a Fourier transform (FT), the Pd extended X-ray  
8 absorption fine structure (EXAFS) spectra (**Figure 1c**) are obtained to determine the local  
9 structures of the Pd species. In reference to standard Pd foil and PdO, Pd-CdS/SiO<sub>2</sub> does not  
10 present the peak in region 2 to 3 Å from the Pd-Pd contribution, suggesting the sole presence of  
11 isolated and dispersed Pd single atoms in Pd-CdS/SiO<sub>2</sub>.<sup>32-33</sup> The only one notable Pd-O  
12 coordination peak in region 1 to 2 Å can be observed in EXAFS spectrum of Pd-CdS/SiO<sub>2</sub>,  
13 which indicates that the single Pd atoms are coordinated with O atoms. Quantitative coordination  
14 structural results for the isolated Pd atoms are extracted from EXAFS curve fitting (**Figure 1d**  
15 and **Table S1**). The coordination number (CN) of the O atoms for individual Pd atoms is  
16 calculated to be 4.1, corroborating the coordinately unsaturated single Pd atoms as compared  
17 with Pd foil (CN = 12) and PdO (CN = 8).<sup>34</sup> In addition, the Ni K-edge XANES spectrum of Ni-  
18 CdS/SiO<sub>2</sub>, featuring the pre-edge and white-line peak similar to the reference spectrum of NiO  
19 (**Figure 1e**), confirms that Ni atoms carry positive charges +2, consistent with the XPS data  
20 (**Figure S10 and S11**).<sup>35</sup> Concerning the FT-EXAFS spectrum of Ni-CdS/SiO<sub>2</sub> (**Figure 1f**),  
21 besides a strong peak centered at about 2.0 Å from Ni-O contribution, another lower shell peak  
22 in the region 2.5 to 3.5 Å is detected, indicating the presence of Ni-O-Ni/Ni-Ni contribution  
23 derived from ultrasmall Ni-oxo clusters,<sup>36</sup> which was further confirmed by the Wavelet  
24 transform plot and EXAFS data fitting results (**Figure S12 and Table S2**). With the further aid  
25 of first principle density functional theory (DFT) optimization calculations, the most stable  
26 structures of Pd-CdS/SiO<sub>2</sub> and Ni-CdS/SiO<sub>2</sub> were verified, as sketched in the insets model of  
27 **Figure 1d and g**.

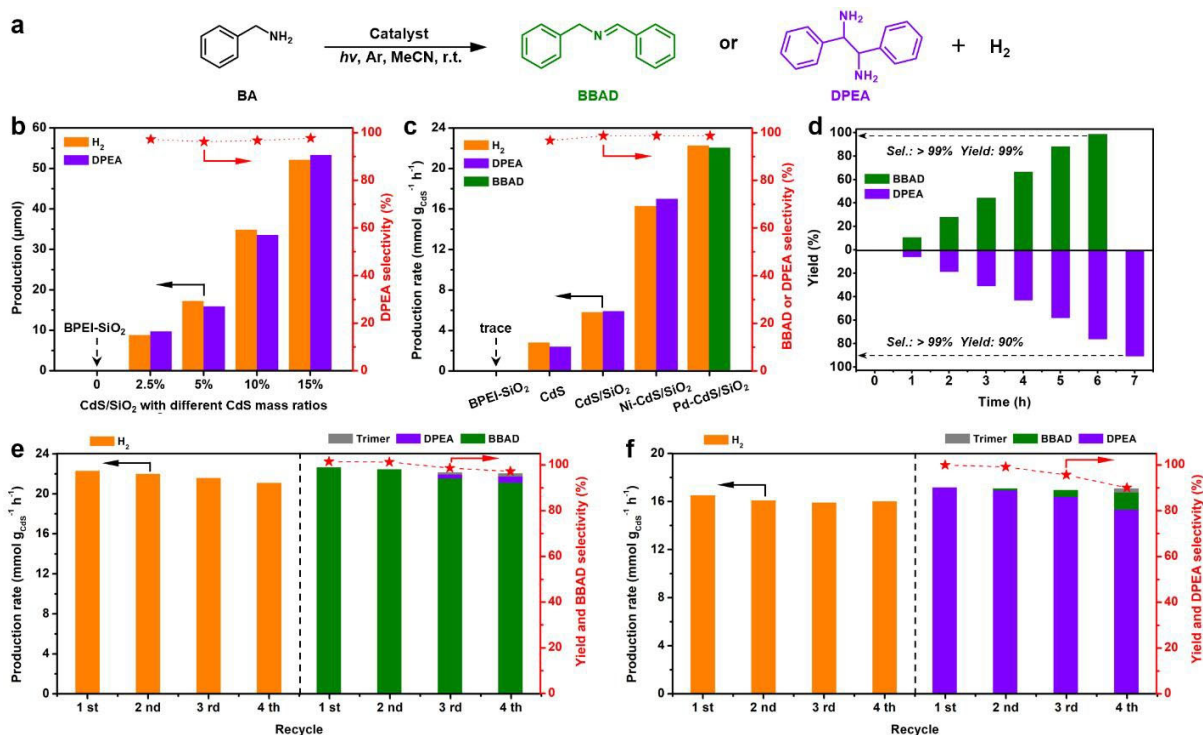


**Figure 2** (a) Schematic representation of the chemical reactions involved in the suggested process for conversion of BA into BBAD or DPEA as well as H<sub>2</sub>. (b) Results from dehydrocoupling of BA to DPEA and H<sub>2</sub> over CdS/SiO<sub>2</sub> composite with different weight contents of CdS QDs after 6 h of xenon-lamp irradiation. (c) Photocatalytic oxidative coupling of BA to DPEA/BBAD and H<sub>2</sub> over different samples. (d) Time profiles of oxidative coupling of BA over Pd-CdS/SiO<sub>2</sub> and Ni-CdS/SiO<sub>2</sub> composite. Recycling performance of (e) Pd-CdS/SiO<sub>2</sub> composite and (f) Ni-CdS/SiO<sub>2</sub> composite toward photocatalytic selective BA oxidation with H<sub>2</sub> production.

### Dehydrocoupling of amines to produce imines or vicinal diamines

N-containing compounds represent a privileged class of bulk commodities and fine chemicals, which are extensively used in pharmaceuticals, fragrances, dyes, fungicides, and agricultural chemicals.<sup>37</sup> Nearly 90% of the top 200 drugs are N-containing derived compounds, and their global market is more than \$50 billion per year.<sup>18</sup> Amines, as well as their derivatives, are among the most versatile building blocks for the synthesis of above application-oriented N-containing chemicals.<sup>38</sup> In the next, we investigated the application of M-CdS/SiO<sub>2</sub> (M=Ni or Pd) for the dehydrocoupling of amines into C–C coupled product of diamines or C–N coupled product of imines in one tunable photoredox catalytic system. Taking benzylamine (BA) as a

model substrate, the dehydrocoupling of BA into N-benzylbenzaldimine (BBAD) or 1,2-diphenylethylenediamine (DPEA) integrated with H<sub>2</sub> production (**Figure 2a**) was carried out in an acetonitrile solution containing 0.2 mmol of BA and 10 mg of the obtained samples, which was irradiated with a xenon lamp at ambient conditions. A linear relationship between the CdS loading amount and the amount of evolved H<sub>2</sub>/DPEA is found, and the optimal DPEA formation amount of 53 μmol can be achieved over 15%-CdS/SiO<sub>2</sub> with a selectivity of above 98% (**Figure 2b**). Upon decorating with Ni, the Ni-CdS/SiO<sub>2</sub> exhibits enhanced H<sub>2</sub> evolution rate by 2.8 times as compared with CdS/SiO<sub>2</sub>; meanwhile, the DPEA formation rate improves from 5.9 to 17.0 mmol g<sub>CdS</sub><sup>-1</sup> h<sup>-1</sup> (**Figure 2c** and **S13a**). Specifically, the decoration of Pd onto CdS/SiO<sub>2</sub> not only boosts the evolution of H<sub>2</sub>, but also tunes the selectivity of BA oxidation from DPEA to BBAD. As a result, over Pd-CdS/SiO<sub>2</sub>, a BBAD formation rate of 22.1 mmol g<sub>CdS</sub><sup>-1</sup> h<sup>-1</sup> can be obtained with a high selectivity of above 99% (**Figure 2c** and **S13b**). The molar ratios of oxidation product (DPEA/BBAD) and reduction product (H<sub>2</sub>) during the reaction, are calculated to be approximately 1.0, suggesting a stoichiometric dehydrocoupling reaction. With irradiation for 6 h, the yield of BBAD over Pd-CdS/SiO<sub>2</sub> reaches 99% (**Figure 2d** and **S14-16**). As for DPEA, a yield of 90% is achieved over Ni-CdS/SiO<sub>2</sub> with the selectivity of above 99% after 7 h. Furthermore, the optimized apparent quantum yield (AQY) of 15.7% for H<sub>2</sub> is achieved at λ = 365 nm (**Figure S17**), which is a competitive photocatalytic system for selective organic transformation or H<sub>2</sub> evolution.

Such covalent-assembly approach of loading CdS QDs onto the SiO<sub>2</sub> support is leading to the recovery and re-dispersion of ultrasmall CdS QDs from the reaction solution for long-term repeated uses. After four repeated trials, the catalytic performance for H<sub>2</sub> and BBAD/DPEA production over M-CdS/SiO<sub>2</sub> (M=Pd or Ni) remains stable (**Figure 2e** and **f**), whereas that of unsupported CdS QDs has diminished by approximately 33% for H<sub>2</sub>, 31% for DPEA (**Figure S18**). A very small amount of trimer (2,4,5-triphenyl-1*H*-imidazole, yield < 2%, **Figure S19**) after three consecutive cycles is obtained over above catalysts, which presumably results from the photocyclization between residual BBAD and newly generated C-centered radical.<sup>39</sup> **Figure S20** and **21** illustrate the well maintenance of crystal structure and element composition in recycled M-CdS/SiO<sub>2</sub>, reflecting a high durability of the covalent assembled M-CdS/SiO<sub>2</sub>. As displayed in **Table S3**, the results of inductively coupled plasma (ICP) spectroscopy analysis evidences that there are slightly detectable Cd<sup>2+</sup> (1.12 μg, corresponding to 0.19% of leaching

ratio) and  $S^{2-}$  (2.18  $\mu\text{g}$ , corresponding to 0.24% of leaching ratio) leakage over CdS/SiO<sub>2</sub> in the reaction solution, which are much lower than those of bare CdS QDs (4.35  $\mu\text{g}$  for Cd<sup>2+</sup>, 7.08  $\mu\text{g}$  for S<sup>2-</sup>). These results signify that this covalent-assembly strategy not only facilitates the recovery of CdS QDs for reuse, but also inhibits the photocorrosion of CdS QDs, thus endowing M-CdS/SiO<sub>2</sub> with excellent durability.

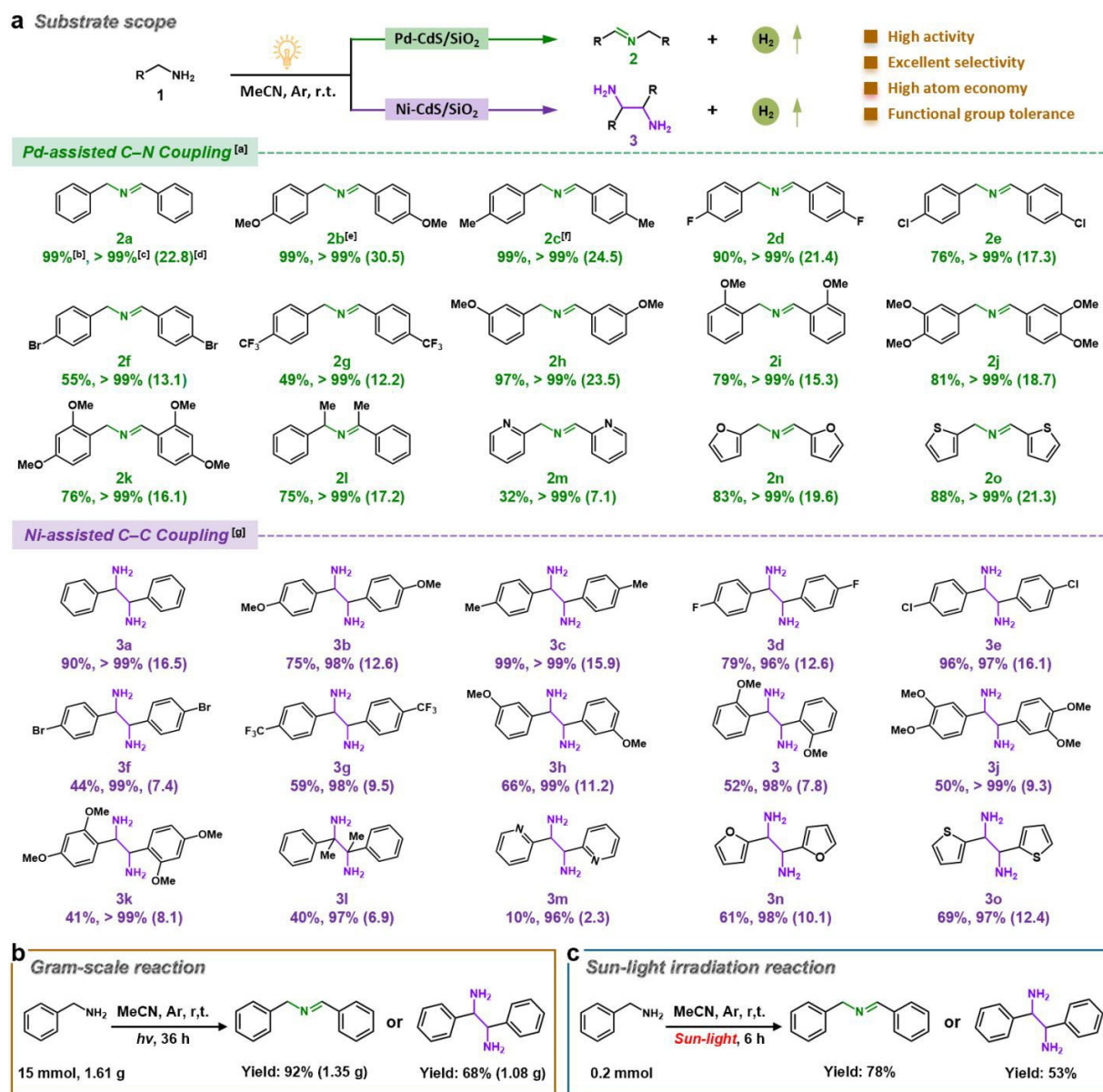


**Figure 3.** (a) Substrate scope of amines. (b) Gram-scale synthesis. (c) Sun-light irradiation reaction. <sup>[a]</sup>Reaction conditions: 0.2 mmol BA, 10 mL CH<sub>3</sub>CN, 10 mg Pd-CdS/SiO<sub>2</sub>, Ar atmosphere, 300 W xenon lamp, 6 h, room temperature. <sup>[b]</sup>Yield (%). <sup>[c]</sup>Selectivity (%). <sup>[d]</sup>H<sub>2</sub>

1  
2  
3 production rate ( $\text{mmol g}_{\text{CdS}}^{-1} \text{h}^{-1}$ ). [e]Reaction time is 4 h. [f]Reaction time is 5 h. [g]Reaction  
4 conditions: 0.2 mmol BA, 10 mL  $\text{CH}_3\text{CN}$ , 10 mg Ni-CdS/SiO<sub>2</sub>. Ar atmosphere, 300 W xenon  
5 lamp, 7 h, room temperature.  
6  
7

### 8 9 **Substrate scope and synthetic applications**

10  
11 Following these initial promising results, we began to evaluate the generality of our  
12 cooperative photoredox-catalysed system for the dehydrogenative coupling of amines into C–N  
13 coupled imines or C–C coupled vicinal diamines integrated with H<sub>2</sub> production. As displayed in  
14 **Figure 3a**, a wide range of aromatic amines bearing different para-substituent groups react  
15 smoothly to afford corresponding amines or vicinal diamines with moderate to excellent yields  
16 as well as outstanding selectivity (> 96%). (2b-2g and 3b-3g). Among them, a strong electron-  
17 withdrawing group, namely trifluoromethyl ( $-\text{CF}_3$ ), is also tolerated, albeit with relatively low  
18 yields (49% for 2g, 59% for 3g). This system is also quite compatible with ortho- and meta-  
19 substituted aromatic amines to deliver the corresponding products in 52%–97% yields (2h-2i and  
20 3h-3i). Dehydrogenative coupling of 3,4(or 2,4)-di-substituted aromatic amines furnishes the  
21 corresponding imines and vicinal diamines with yields of 81% (2j, 76% for 2k) and 50% (3j,  
22 41% for 3k), respectively. In the case of  $\alpha$ -methylbenzylamine, the desired products 2l and 3l are  
23 obtained in moderate yields of 75% and 40%, respectively. It is noteworthy that this current  
24 system is also applicable to heteroatom-containing amines (1m-1o), which usually have  
25 detrimental effects (*i.e.*, catalyst poisoning caused by the strong coordination of amines to the  
26 metal center) on the activity and stability of metal-complex catalysts,<sup>40</sup> although a slight drop in  
27 yields is observed (2m-2o and 3m-3o) compared with benzylic amines.  
28  
29  
30  
31  
32  
33  
34  
35  
36  
37  
38  
39  
40

41 Compared with previous reports on the synthesis of imines and vicinal diamines (**Table S4**  
42 and **S5**), the present system not only bypasses the use of additional chemical reagents, but also  
43 releases stoichiometric H<sub>2</sub> as green fuel. In addition, this catalytic system is the first report of  
44 solar-driven dehydrocoupling of amines to vicinal diamines. More importantly, the catalytic  
45 performance over M-CdS/SiO<sub>2</sub> is superior to that of the previously reported catalyst systems. As  
46 a proof-of-concept, this catalytic system was evaluated to synthesize BBAD and DPEA on a  
47 gram scale. Consequently, a BBAD yield of 92% (1.35 g) and a DPEA yield of 68% (1.08 g)  
48 within 36 h are obtained over Pd-CdS/SiO<sub>2</sub> and Ni-CdS/SiO<sub>2</sub>, respectively (**Figure 3b**). Even  
49 more, the desired product BBAD and DPEA can be obtained with the yields of 78% and 53%,  
50  
51  
52  
53  
54  
55  
56  
57  
58  
59  
60

respectively, upon direct irradiation by natural sunlight (**Figure 3c**). These results demonstrate the feasibility and potential of this SiO<sub>2</sub>-supported M-CdS QDs protocol in practical synthesis.

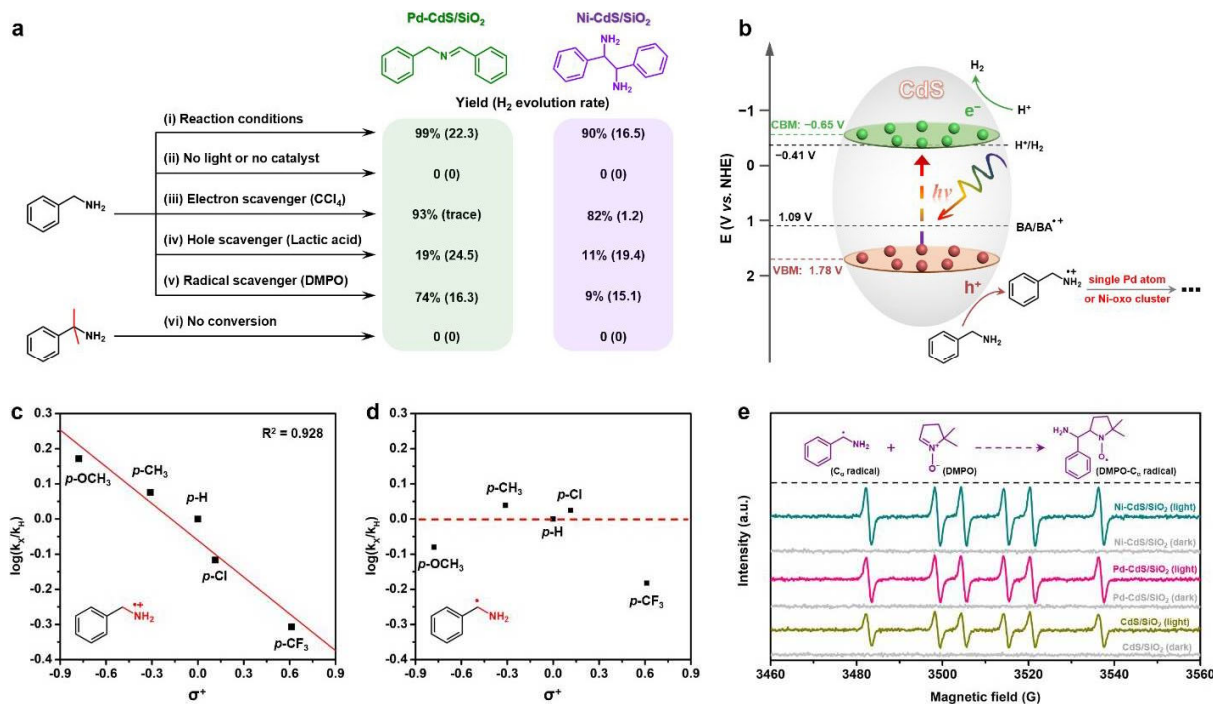


**Figure 4.** (a) Control experiments and quenching experiments with different additives catalysed by Ni-CdS/SiO<sub>2</sub> and Pd-CdS/SiO<sub>2</sub> composite. Scavenger concentrations: 20 mM CCl<sub>4</sub>, Lactic acid or DMPO. Reaction time: 6 h. (b) Redox potentials of oxidative dehydrogenation of BA and H<sub>2</sub> evolution against the positions of VBM and CBM of CdS QDs. Hammett plots for the selective oxidation of para-substituted benzylamines coupled with H<sub>2</sub> production over (c) Pd-CdS/SiO<sub>2</sub> and (d) Ni-CdS/SiO<sub>2</sub> composite. (e) *In-situ* EPR spectra of CdS/SiO<sub>2</sub>, Ni-CdS/SiO<sub>2</sub> and Pd-CdS/SiO<sub>2</sub> composite in Ar saturated CH<sub>3</sub>CN solution in the presence of DMPO.

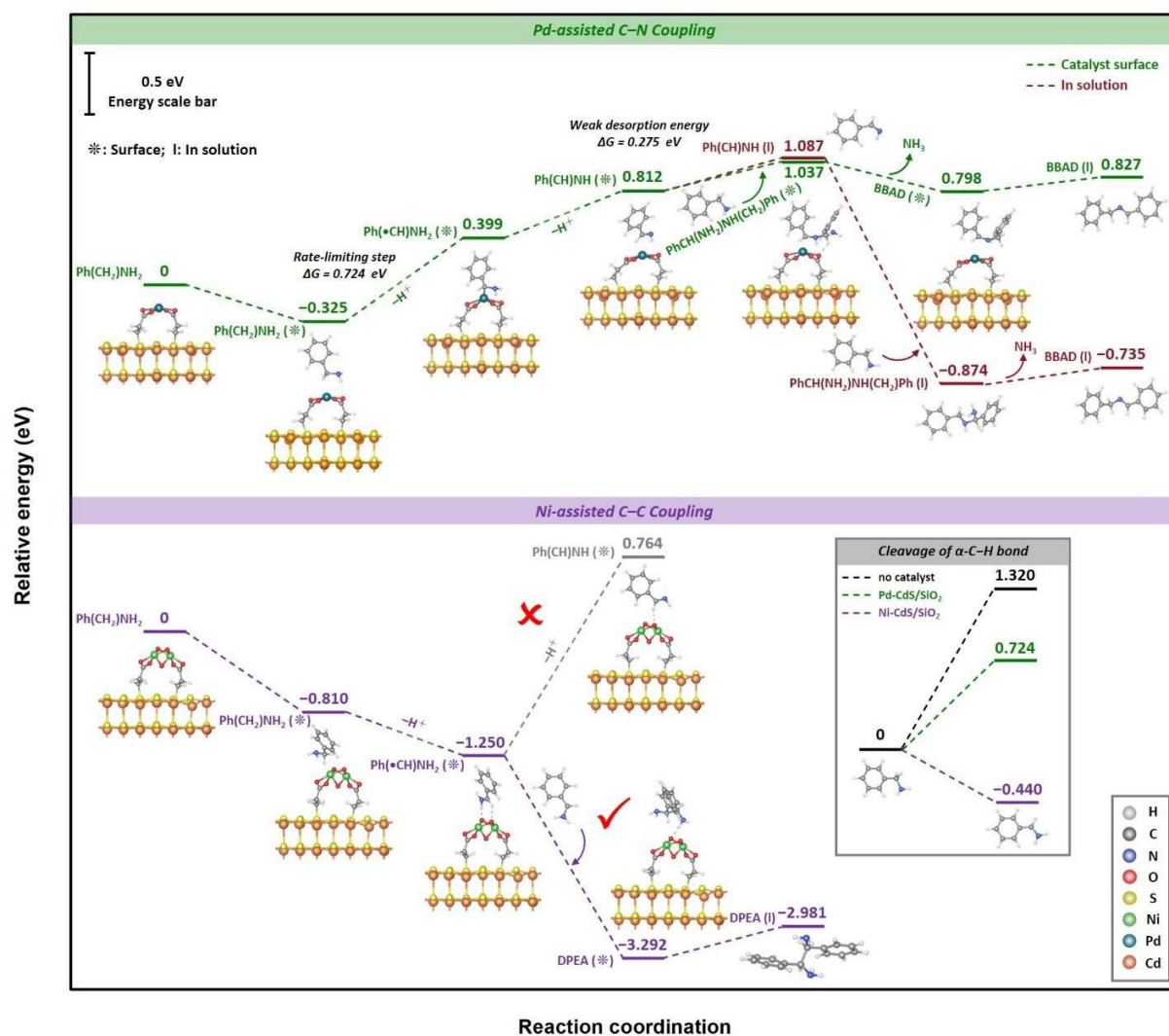
### Mechanism insight for dehydrocoupling of amines

To probe the reaction mechanism for the dehydrocoupling of amines integrated with H<sub>2</sub> production in the present catalytic system, we first performed a series of control and quenching experiments, as displayed in **Figure 4a**. Control experiments imply that, in the absence of light or catalysts, the reaction cannot proceed at all (**Figure 4a (ii)**). The addition of CCl<sub>4</sub> as electron scavenger completely ceased the H<sub>2</sub> evolution, and moreover, the formation of BBAD/DPEA was retarded once introducing lactic acid (**Figure 4a (iii) and (iv)**), suggesting the joint participation of electrons and holes for H<sub>2</sub> and BBAD/DPEA production. Based on the Tauc plot

(**Figure S22**), the bandgap ( $E_g$ ) of CdS QDs is evaluated to be 2.43 eV. The conduction band minimum (CBM) of CdS is estimated at  $-0.65$  V vs normal hydrogen electrode (NHE) according to the Mott–Schottky analysis, and the valance band maximum (VBM) of CdS is thus calculated with the value of  $1.78$  V vs NHE. Moreover, the redox potential of BA is measured to be about  $1.09$  V vs NHE according to the cyclic voltammograms (**Figure S23**). Thermodynamic constraints require that, for these two half-reactions to proceed simultaneously, the CBM of CdS QDs needs to be more negative than  $H^+/H_2$  energy level ( $-0.41$  V vs NHE), whereas the VBM must have a more positive potential than  $BA/BA^{*+}$  energy level ( $1.09$  V vs NHE).<sup>12</sup> As sketched in **Figure 4b**, upon light irradiation, the charge carriers, *i.e.*, electron-hole pairs, are generated from the photoexcitation of CdS QDs; and the loading of Ni or Pd cocatalyst significantly expedites photoinduced charge carrier separation, as evidenced by **Figure S24**, which results in a significantly enhanced activity. The photoexcited holes with sufficient thermodynamic driving force can readily oxidize BA into its cationic form for subsequent coupling reaction; meanwhile, the abstracted protons are reduced by photoexcited electrons to produce  $H_2$ .

To further decipher the catalytic mechanism for the selectivity regarding divergent synthesis of BBAD and DPEA over M-CdS/SiO<sub>2</sub>, the radical-quenching experiment has been conducted. The addition of 5,5-dimethyl-1-pyrrolineN-oxide (DMPO) as a radical scavenger significantly suppresses the formation of DPEA over Ni-CdS/SiO<sub>2</sub>, but only slightly retards the BBAD production over Pd-CdS/SiO<sub>2</sub> (**Figure 4a (v)**), which preliminarily reveals that the generation of two kinds of homo-coupling products follows different intermediates-mediated pathways. In addition, the reaction for cumylamine dehydrogenation completely stops (**Figure 4a (vi)**), suggesting that the cleavage of  $\alpha$ -C–H bond is crucial to the reaction. To identify the rate-limiting step of BBAD/DPEA formation, we examined the  $\alpha$ -C–H bond activation in BA by graphing the Hammett plot. A reasonable linearity between the  $\log(k_X/k_H)$  values and the Brown–Okamoto constants ( $\sigma^+$ ) is obtained over Pd-CdS/SiO<sub>2</sub> (**Figure 4c**), suggesting that the dehydrocoupling of BA proceeds *via* the intermediacy of a cationic species ( $PhCH_2NH_2^{*+}$ ), and  $\alpha$ -C–H bond cleavage is the rate-limiting step in the formation of BBAD.<sup>41–43</sup> However, for the synthesis of DPEA over Ni-CdS/SiO<sub>2</sub>, para-substituted benzylamines show irregular and marginal influence on the reaction rates (**Figure 4d**), confirming a neutral C-centered radical (*i.e.*,  $Ph(\bullet CH)NH_2$ ) involved in the reaction.<sup>41, 44</sup> Furthermore, *in-situ* electron paramagnetic resonance (EPR) spectroscopy was performed to monitor the effect of Pd or Ni cocatalyst in the

dehydrocoupling of amines (**Figure 4e** and **S25**). Upon light irradiation,  $\text{Ph}(\bullet\text{CH})\text{NH}_2$  is gradually evolved over all catalysts and eventually trapped by DMPO, as evidenced by the characteristic signal peaks belonging to the DMPO- $\text{PhCHNH}_2$  adduct (**Figure S25** and **S26**).<sup>43</sup> Upon Pd or Ni decoration, an obvious increase in the evolution rate of  $\text{Ph}(\bullet\text{CH})\text{NH}_2$  radical is observed, indicating that both Pd and Ni species significantly promote the deprotonation of amines. It is worth noting that Pd-CdS/SiO<sub>2</sub> exhibits the optimal catalytic performance for the dehydrocoupling of BA (**Figure 2c**); however, the evolution rate of  $\text{Ph}(\bullet\text{CH})\text{NH}_2$  radical over Pd-CdS/SiO<sub>2</sub> is obviously lower than that of Ni-CdS/SiO<sub>2</sub>, which further indicates that the cleavage of  $\alpha\text{-C-H}$  bond is a rate-limiting step in Pd-assisted catalytic system.



1  
2  
3 **Figure 5.** Calculated potential energy diagrams for dehydrocoupling of BA to BBAD or DPEA  
4 catalysed by the M-CdS/SiO<sub>2</sub> composite. Inset in **Figure 5** is the cleavage energy comparison of  
5  $\alpha$ -C–H bond under different conditions.  
6  
7  
8

9  
10 Upon gathering the above information, we can conclude that the cleavage of  $\alpha$ -C–H bond is  
11 a rate-limiting step in Pd-assisted catalytic system for BBAD formation process over Pd-  
12 CdS/SiO<sub>2</sub>, whereas homo-coupling of Ph( $\bullet$ CH)NH<sub>2</sub> is the key step in the Ni-assisted catalytic  
13 system for DPEA formation process over Ni-CdS/SiO<sub>2</sub>. To further gain insights into the  
14 selectivity regulation and the overall reaction pathways for the dehydrocoupling of BA over Pd-  
15 CdS/SiO<sub>2</sub> and Ni-CdS/SiO<sub>2</sub>, density functional theory (DFT) calculations were performed.  
16  
17 According to EXAFS analysis, a single Pd atom and two-atom Ni cluster coordinated with MPA  
18 on the surface of cubic CdS QDs were constructed to represent the active sites on Pd-CdS/SiO<sub>2</sub>  
19 and Ni-CdS/SiO<sub>2</sub>, respectively (**Figure S28** and **S29**). As depicted in **Figure 5**, both BA  
20 adsorption steps over Pd-CdS/SiO<sub>2</sub> and Ni-CdS/SiO<sub>2</sub> composite are exothermic with the values  
21 of  $-0.325$  and  $-0.810$  eV, respectively. The first deprotonation step of BA\* over Pd-CdS/SiO<sub>2</sub> is  
22 endergonic by a high energy barrier of  $0.724$  eV (that for the case without catalyst is  $1.320$  eV,  
23 inset in **Figure 5**), suggesting that the activation of C–H bond in BA is a rate-limiting step for  
24 BA dehydrocoupling occurs on Pd-CdS/SiO<sub>2</sub> consistent with the conclusion drawn from the  
25 experimental data; nevertheless, such deprotonation process is spontaneous on the surface of Ni-  
26 CdS/SiO<sub>2</sub> with the C–H bond dissociation energy of  $-0.44$  eV. For the Pd-assisted BBAD  
27 formation mechanism, the formed Ph( $\bullet$ CH)NH<sub>2</sub> radical can be further protonated to produce a  
28 highly active aldimine intermediate (*i.e.*, (phenyl)methanimine) by overcoming a moderate  
29 energy barrier of  $0.413$  eV. Subsequently, the aldimine intermediate is prone to undergo an  
30 addition-elimination mechanism,<sup>45</sup> *i.e.*, the addition of another BA molecule to form N-benzyl-1-  
31 phenylmethanediamine, thereby ensuring elimination of ammonia (**Figure S27**) for BBAD  
32 production. Considering the weak (phenyl)methanimine desorption energy of  $0.275$  eV on the  
33 Pd-CdS/SiO<sub>2</sub> surface, a thermodynamically more feasible reaction pathway is that, the aldimine  
34 intermediate is preferentially desorbed from the surface of Pd-CdS/SiO<sub>2</sub> to the solution,  
35 undertaking a thermodynamically downhill addition-elimination pathway with an exergonic  
36 condensation energy of  $-1.961$  eV, followed by a very low elimination energy of  $0.139$  eV to  
37 produce BBAD (**Figure S30**). In contrast, as for the Ni-assisted DPEA formation mechanism, it  
38 is noteworthy that the second deprotonation process of Ph( $\bullet$ CH)NH<sub>2</sub> radical is significantly  
39  
40  
41  
42  
43  
44  
45  
46  
47  
48  
49  
50  
51  
52  
53  
54  
55  
56  
57  
58  
59  
60

harder thermodynamically due to the high N–H bond cleavage energy of 2.014 eV. In such a scenario, a homo-coupling pathway for DPEA production is thermodynamically favorable with an exergonic energy of  $-2.042$  eV, which is considered to be the critical step to tune the product selectivity. Hence, the theoretical studies of BA dehydrocoupling reveal that the divergent synthesis of BBAD and DPEA over M-CdS/SiO<sub>2</sub> originates from the reasonable C–H/N–H bond cleavage energy on the Pd-CdS/SiO<sub>2</sub> surface and a large exergonic C–C coupling energy enabled by Ni-CdS/SiO<sub>2</sub>. Taking the above experimental and theoretical results together, the overall catalytic reaction mechanism has been proposed accordingly in **Figure 6**.

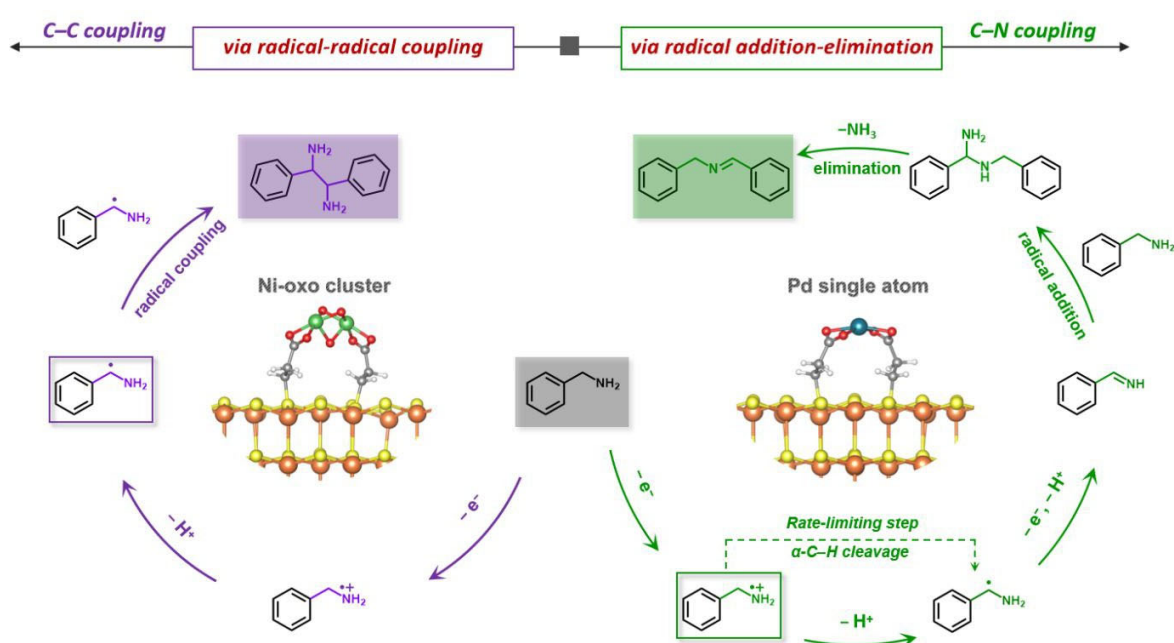


**Figure 6.** Proposed mechanism for dehydrocoupling of BA to BBAD or DPEA catalysed by the M-CdS/SiO<sub>2</sub> composite.

## Conclusions

In summary, we report the strategy of designing the structurally well-defined cocatalyst over the semiconductor surface to steer unselective photogenerated radicals for the tunable selective photoredox dehydrocoupling of amines into C–C coupled vicinal diamines or C–N coupled imines concomitantly with H<sub>2</sub> byproduct over the atomically dispersed Ni or Pd-decorated CdS/SiO<sub>2</sub> composite. Our methodology is compatible with a variety of readily available amines, affording the high-performance production of vicinal diamines and imines with outstanding selectivity, stability and recyclability. Mechanistic studies confirm the Ph( $\bullet$ CH)NH<sub>2</sub>

1  
2  
3 and  $\text{PhCH}_2\text{NH}_2^{*+}$  as dominant radical intermediates for the divergent synthesis of C–C coupled  
4  
5 vicinal diamines and C–N coupled imines, respectively, as enabled by specific cocatalyst of Ni-  
6  
7 oxo cluster and single Pd atom. This work overcomes the well-known pervasive shortcomings of  
8  
9 selectivity regulation in semiconductor-based heterogeneous photochemical synthesis, and is  
10  
11 expected to pave the way of decorating atomically dispersed cocatalysts as the active sites onto  
12  
13 semiconductor to maneuver radical conversion for divergent synthesis of fine chemicals.

## 14 15 16 **Methods**

17  
18 **Synthesis of EDC/NHS covalent assembled CdS/SiO<sub>2</sub>.** In a typical process, 0.1 g of BPEI-  
19  
20 SiO<sub>2</sub> was mixed with 0.1 g of NHS and 1 mL of EDC in 100 mL of phosphate buffer saline (pH  
21  
22 = 7.0), which was kept at an ambient temperature with stirring for 15 min. A certain  
23  
24 concentration of CdS QDs was then added into the above solution, stirred for another 6 h.  
25  
26 Afterwards, the as-synthesized samples were isolated by centrifugation, followed by drying at 60  
27  
28 °C in an oven. The obtained products are labeled as x%CdS/SiO<sub>2</sub>, in which x% (x = 2.5, 5, 10  
29  
30 and 15) stands for the mass ratio of CdS QDs.

31  
32 **Synthesis of M-CdS/SiO<sub>2</sub>.** M-CdS/SiO<sub>2</sub> was prepared based on a facile photodeposition  
33  
34 strategy. Typically, 50 mg of CdS/SiO<sub>2</sub> was dissolved in a 50 mL of mixed solution of DI water  
35  
36 (40 mL) and ethanol (10 mL) that contained a certain amount of PdCl<sub>2</sub>. Subsequently, the  
37  
38 suspension was irradiated with UV-vis light ( $\lambda > 300$  nm) under nitrogen (N<sub>2</sub>) atmosphere for 0.5  
39  
40 h. The obtained products were collected *via* centrifugation and washed by DI water. Followed by  
41  
42 blow-drying with N<sub>2</sub>, the Pd-CdS/SiO<sub>2</sub> composites with different Pd weight loading (0.15%,  
43  
44 0.3%, 0.75% and 1.5%) were obtained. The photodeposition of Ni cocatalyst for the synthesis of  
45  
46 Ni-CdS/SiO<sub>2</sub> composites with different Ni weight loading (0.3%, 0.75%, 1.5% and 2%) takes the  
47  
48 same method, except for the difference of precursor (NiCl<sub>2</sub>·6H<sub>2</sub>O for Ni).

49  
50 **Photoactivity testing.** Photocatalytic H<sub>2</sub> evolution paired with imine or vicinal diamine  
51  
52 synthesis was carried out in a double-walled quartz reactor, which was maintained at 25 °C by a  
53  
54 flow of circulating water. Typically, 10 mg sample was added into 10 mL CH<sub>3</sub>CN containing 0.2  
55  
56 mmol amines. The reaction solution was purged with Ar gas for 20 min. Then, a 300 W xenon  
57  
58 lamp (PLS-SXE 300D, Beijing Perfectlight Co., Ltd.) was used as light source, and the light  
59  
60 power density is measured to be approximately 120 mW cm<sup>-2</sup>. The generated H<sub>2</sub> was quantified  
by a gas chromatograph (Shimadzu GC-8A 2014C). The liquid products were analyzed by the  
gas chromatography-mass spectrometry (Shimadzu GC-MS QP 2020, Q-Exactive, see **Figure**  
**S16** and **S31-44** for the corresponding Mass spectra).

## 51 52 ASSOCIATED CONTENT

### 53 54 **Supporting Information.**

55  
56  
57  
58  
59  
60 The Supporting Information is available free of charge at <http://pubs.acs.org>.

1  
2  
3 Additional experimental details, characterization (crystal structures, morphologies, and optical  
4 absorption properties) and photoactivity results of the obtained sample. Energy band structure of  
5 CdS QDs, photoelectrochemical measurements of various samples, additional DFT results. Mass  
6 spectra of the obtain liquid-products.  
7  
8  
9

## 10 AUTHOR INFORMATION

### 11 12 13 **Corresponding Author**

14 **Yi-Jun Xu** — College of Chemistry, State Key Laboratory of Photocatalysis on Energy and  
15 Environment, Fuzhou University, Fuzhou, 350116, China; orcid.org/0000-0002-2195-1695;  
16 Email: yjxu@fzu.edu.cn; Homepage: <http://xugroup.fzu.edu.cn>.  
17  
18  
19

### 20 **Author Contributions**

21 Y.-J.X. proposed the research direction and supervised the project. M.-Y.Q. designed and  
22 preformed the experiments. Y.-J.X. and M.-Y.Q. wrote and revised the manuscript. Z.-R.T. and  
23 M.C. provided helpful suggestions. All authors participated in discussion and reviewed the paper  
24 before submission.  
25  
26  
27  
28  
29

### 30 **Notes**

31 The authors declare no competing financial interest.  
32  
33

## 34 ACKNOWLEDGMENT

35 This work was supported by the Natural Science Foundation of China (22172030, 22072023,  
36 21872029, U1463204 and 21173045), the Program for National Science and Technology  
37 Innovation Leading Talents (00387072), the Program for Leading Talents of Fujian Universities,  
38 the 1st Program of Fujian Province for Top Creative Young Talents, and the Natural Science  
39 Foundation of Fujian Province (2017J07002 and 2019J01631).  
40  
41  
42  
43  
44  
45  
46

## 47 REFERENCES

- 48 (1) Moran, J.; Preetz, A.; Mesch, R. A.; Krische, M. J. Iridium-catalysed direct C-C coupling of  
49 methanol and allenes. *Nat. Chem.* **2011**, *3*, 287-290.  
50
- 51 (2) Wang, H.; Gao, X.; Lv, Z.; Abdelilah, T.; Lei, A. Recent advances in oxidative R<sup>1</sup>-H/R<sup>2</sup>-H  
52 cross-coupling with hydrogen evolution via photo-/electrochemistry. *Chem. Rev.* **2019**, *119*,  
53 6769-6787.  
54  
55  
56  
57  
58  
59  
60

1  
2  
3 (3) Hazari, N.; Melvin, P. R.; Beromi, M. M. Well-defined nickel and palladium precatalysts  
4 for cross-coupling. *Nat. Rev. Chem.* **2017**, *1*, 0025.

5  
6  
7 (4) Hu, A.; Guo, J.-J.; Pan, H.; Tang, H.; Gao, Z.; Zuo, Z.  $\delta$ -Selective Functionalization of  
8 Alkanols Enabled by Visible-Light-Induced Ligand-to-Metal Charge Transfer. *J. Am. Chem.*  
9 *Soc.* **2018**, *140*, 1612-1616.

10  
11  
12 (5) Marzo, L.; Pagire, S. K.; Reiser, O.; Koenig, B. Visible-light photocatalysis: does It make a  
13 difference in organic synthesis? *Angew. Chem. Int. Ed.* **2018**, *57*, 10034-10072.

14  
15 (6) Musacchio, A. J.; Nguyen, L. Q.; Beard, G. H.; Knowles, R. R. Catalytic Olefin  
16 Hydroamination with Aminium Radical Cations: A Photoredox Method for Direct C-N Bond  
17 Formation. *J. Am. Chem. Soc.* **2014**, *136*, 12217-12220.

18  
19 (7) Trowbridge, A.; Reich, D.; Gaunt, M. J. Multicomponent synthesis of tertiary alkylamines  
20 by photocatalytic olefin-hydroaminoalkylation. *Nature* **2018**, *561*, 522-527.

21  
22 (8) Schultz, D. M.; Yoon, T. P. Solar synthesis: prospects in visible light photocatalysis.  
23  
24  
25 *Science* **2014**, *343*, 1239176.

26  
27 (9) Cui, X.; Li, W.; Ryabchuk, P.; Junge, K.; Beller, M. Bridging homogeneous and  
28 heterogeneous catalysis by heterogeneous single-metal-site catalysts. *Nat. Catal* **2018**, *1*, 385-  
29 397.

30  
31 (10) Jiang, Y.; Lopez-Arteaga, R.; Weiss, E. A. Quantum Dots Photocatalyze Intermolecular  
32 2+2 Cycloadditions of Aromatic Alkenes Adsorbed to their Surfaces via van der Waals  
33 Interactions. *J. Am. Chem. Soc.* **2022**, *144*, 3782-3786.

34  
35 (11) Caputo, J. A.; Frenette, L. C.; Zhao, N.; Sowers, K. L.; Krauss, T. D.; Weix, D. J. General  
36 and efficient C-C bond forming photoredox catalysis with semiconductor quantum dots. *J. Am.*  
37 *Chem. Soc.* **2017**, *139*, 4250-4253.

38  
39 (12) Qi, M.-Y.; Conte, M.; Anpo, M.; Tang, Z.-R.; Xu, Y.-J. Cooperative coupling of oxidative  
40 organic synthesis and hydrogen production over semiconductor-based photocatalysts. *Chem.*  
41 *Rev.* **2021**, *121*, 13051-13085.

42  
43 (13) Kou, J.; Lu, C.; Wang, J.; Chen, Y.; Xu, Z.; Varma, R. S. Selectivity Enhancement in  
44 Heterogeneous Photocatalytic Transformations. *Chem. Rev.* **2017**, *117*, 1445-1514.

45  
46 (14) Gao, C.; Low, J.; Long, R.; Kong, T.; Zhu, J.; Xiong, Y. Heterogeneous Single-Atom  
47 Photocatalysts: Fundamentals and Applications. *Chem. Rev.* **2020**, *120*, 12175-12216.

1  
2  
3 (15) Ji, S.; Chen, Y.; Zhao, S.; Chen, W.; Shi, L.; Wang, Y.; Dong, J.; Li, Z.; Li, F.; Chen, C.;  
4 Peng, Q.; Li, J.; Wang, D.; Li, Y. Atomically Dispersed Ruthenium Species Inside Metal-  
5 Organic Frameworks: Combining the High Activity of Atomic Sites and the Molecular Sieving  
6 Effect of MOFs. *Angew. Chem. Int. Ed.* **2019**, *58*, 4271-4275.

7  
8  
9 (16) Liu, Z.; Huang, F.; Peng, M.; Chen, Y.; Cai, X.; Wang, L.; Hu, Z.; Wen, X.; Wang, N.;  
10 Xiao, D.; Jiang, H.; Sun, H.; Liu, H.; Ma, D. Tuning the selectivity of catalytic nitriles  
11 hydrogenation by structure regulation in atomically dispersed Pd catalysts. *Nat. Commun.* **2021**,  
12 *12*, 6194.

13  
14  
15 (17) Wang, L.; Zhang, W.; Wang, S.; Gao, Z.; Luo, Z.; Wang, X.; Zeng, R.; Li, A.; Li, H.;  
16 Wang, M.; Zheng, X.; Zhu, J.; Zhang, W.; Ma, C.; Si, R.; Zeng, J. Atomic-level insights in  
17 optimizing reaction paths for hydroformylation reaction over Rh/CoO single-atom catalyst. *Nat.*  
18 *Commun.* **2016**, *7*, 14036.

19  
20  
21 (18) Jagadeesh, R. V.; Murugesan, K.; Alshammari, A. S.; Neumann, H.; Pohl, M.-M.; Radnik,  
22 J.; Beller, M. MOF-derived cobalt nanoparticles catalyze a general synthesis of amines. *Science*  
23 **2017**, *358*, 326-332.

24  
25 (19) Froidevaux, V.; Negrell, C.; Caillol, S.; Pascault, J.-P.; Boutevin, B. Biobased Amines:  
26 From Synthesis to Polymers; Present and Future. *Chem. Rev.* **2016**, *116*, 14181-14224.

27  
28 (20) Murugesan, K.; Senthamarai, T.; Chandrashekhar, V. G.; Natte, K.; Kamer, P. C. J.; Beller,  
29 M.; Jagadeesh, R. V. Catalytic reductive aminations using molecular hydrogen for synthesis of  
30 different kinds of amines. *Chem. Soc. Rev.* **2020**, *49*, 6273-6328.

31  
32 (21) Zhang, N.; Han, C.; Xu, Y.-J.; Foley, J. J.; Zhang, D.; Codrington, J.; Gray, S. K.; Sun, Y.  
33 Near-field dielectric scattering promotes optical absorption by platinum nanoparticles. *Nat.*  
34 *Photonics* **2016**, *10*, 473-482.

35  
36 (22) Han, C.; Li, S.-H.; Tang, Z.-R.; Xu, Y.-J. Tunable plasmonic core-shell heterostructure  
37 design for broadband light driven catalysis. *Chem. Sci.* **2018**, *9*, 8914-8922.

38  
39 (23) Qi, M.-Y.; Li, Y.-H.; Anpo, M.; Tang, Z.-R.; Xu, Y.-J. Efficient photoredox-mediated C-C  
40 coupling organic synthesis and hydrogen production over engineered semiconductor quantum  
41 dots. *ACS Catal.* **2020**, *10*, 14327-14335.

42  
43 (24) Fereiro, J. A.; Porat, G.; Bendikov, T.; Pecht, I.; Sheves, M.; Cahen, D. Protein electronics:  
44 chemical modulation of contacts control energy level alignment in gold-azurin-gold junctions. *J.*  
45 *Am. Chem. Soc.* **2018**, *140*, 13317-13326.

1  
2  
3 (25) Gannett, P. M.; Kabulski, J.; Perez, F. A.; Liu, Z. Y.; Lederman, D.; Locuson, C. W.;  
4 Ayscue, R. R.; Thomsen, N. M.; Tracy, T. S. Preparation, characterization, and substrate  
5 metabolism of gold-immobilized cytochrome P4502C9. *J. Am. Chem. Soc.* **2006**, *128*, 8374-  
6 8375.

7  
8  
9  
10 (26) D'Ambrosio, E. A.; Bersch, K. L.; Lauro, M. L.; Grimes, C. L. Differential peptidoglycan  
11 recognition assay using varied surface presentations. *J. Am. Chem. Soc.* **2020**, *142*, 10926-10930.

12  
13 (27) Cui, X. F.; Wang, J.; Liu, B.; Ling, S.; Long, R.; Xiong, Y. J. Turning Au nanoclusters  
14 catalytically active for visible-light-driven CO<sub>2</sub> reduction through bridging ligands. *J. Am. Chem.*  
15 *Soc.* **2018**, *140*, 16514-16520.

16  
17 (28) Cecchet, F.; Pilling, M.; Hevesi, L.; Schergna, S.; Wong, J. K. Y.; Clarkson, G. J.; Leigh,  
18 D. A.; Rudolf, P. Grafting of benzylic amide macrocycles onto acid-terminated self-assembled  
19 monolayers studied by XPS, RAIRS, and contact angle measurements. *J. Phys. Chem. B* **2003**,  
20 *107*, 10863-10872.

21  
22 (29) Pippig, F.; Sarghini, S.; Hollaender, A.; Paulussen, S.; Terryn, H. TFAA chemical  
23 derivatization and XPS. Analysis of OH and NH<sub>x</sub> polymers. *Surf. Interface Anal.* **2009**, *41*, 421-  
24 429.

25  
26 (30) Whelan, C. M.; Cecchet, F.; Baxter, R.; Zerbetto, F.; Clarkson, G. J.; Leigh, D. A.; Rudolf,  
27 P. Adsorption of a benzylic amide macrocycle on a solid substrate: XPS and HREELS  
28 characterization of thin films grown on Au(111). *J. Phys. Chem. B* **2002**, *106*, 8739-8746.

29  
30 (31) Wei, S. J.; Li, A.; Liu, J. C.; Li, Z.; Chen, W. X.; Gong, Y.; Zhang, Q. H.; Cheong, W. C.;  
31 Wang, Y.; Zheng, L. R.; Xiao, H.; Chen, C.; Wang, D. S.; Peng, Q.; Gu, L.; Han, X. D.; Li, J.;  
32 Li, Y. D. Direct observation of noble metal nanoparticles transforming to thermally stable single  
33 atoms. *Nat. Nanotechnol.* **2018**, *13*, 856-861.

34  
35 (32) Liu, P.; Zhao, Y.; Qin, R.; Mo, S.; Chen, G.; Gu, L.; Chevrier, D. M.; Zhang, P.; Guo, Q.;  
36 Zang, D.; Wu, B.; Fu, G.; Zheng, N. Photochemical route for synthesizing atomically dispersed  
37 palladium catalysts. *Science* **2016**, *352*, 797-801.

38  
39 (33) Chen, Z.; Vorobyeva, E.; Mitchell, S.; Fako, E.; Ortuno, M. A.; Lopez, N.; Collins, S. M.;  
40 Midgley, P. A.; Richard, S.; Vile, G.; Perez-Ramirez, J. A heterogeneous single-atom palladium  
41 catalyst surpassing homogeneous systems for Suzuki coupling. *Nat. Nanotechnol.* **2018**, *13*, 702-  
42 707

1  
2  
3 (34) Gao, C.; Chen, S.; Wang, Y.; Wang, J.; Zheng, X.; Zhu, J.; Song, L.; Zhang, W.; Xiong, Y.  
4 Heterogeneous single-atom catalyst for visible-light-driven high-turnover CO<sub>2</sub> reduction: the role  
5 of electron transfer. *Adv. Mater.* **2018**, *30*, 1704624.  
6

7  
8 (35) Xia, C.; Qiu, Y.; Xia, Y.; Zhu, P.; King, G.; Zhang, X.; Wu, Z.; Kim, J. Y.; Cullen, D. A.;  
9 Zheng, D.; Li, P.; Shakouri, M.; Heredia, E.; Cui, P.; Alshareef, H. N.; Hu, Y.; Wang, H. General  
10 synthesis of single-atom catalysts with high metal loading using graphene quantum dots. *Nat.*  
11 *Chem.* **2021**, *13*, 887-894.  
12

13  
14 (36) Si, X.; Chen, J.; Lu, F.; Liu, X.; Ren, Y.; Lu, R.; Jiang, H.; Liu, H.; Miao, S.; Zhu, Y.; Luo,  
15 X.; Xu, J. Immobilized Ni clusters in mesoporous aluminum silica nanospheres for catalytic  
16 hydrogenolysis of lignin. *ACS Sustainable Chem. Eng* **2019**, *7*, 19034-19041.  
17

18  
19 (37) Rigoli, J. W.; Weatherly, C. D.; Alderson, J. M.; Vo, B. T.; Schomaker, J. M. Tunable,  
20 chemoselective amination via silver catalysis. *J. Am. Chem. Soc.* **2013**, *135*, 17238-17241.  
21

22  
23 (38) Mukherjee, A.; Nerush, A.; Leitus, G.; Shimon, L. J. W.; Ben David, Y.; Jalapa, N. A. E.;  
24 Milstein, D. Manganese-catalyzed environmentally benign dehydrogenative coupling of alcohols  
25 and amines to form aldimines and H<sub>2</sub>: a catalytic and mechanistic study. *J. Am. Chem. Soc.* **2016**,  
26 *138*, 4298-4301.  
27

28  
29 (39) Wang, M.; Li, L.; Lu, J.; Luo, N.; Zhang, X.; Wang, F. Photocatalytic coupling of amines  
30 to imidazoles using a Mo-ZnIn<sub>2</sub>S<sub>4</sub> catalyst. *Green Chem.* **2017**, *19*, 5172-5177.  
31

32  
33 (40) Lang, X.; Ma, W.; Zhao, Y.; Chen, C.; Ji, H.; Zhao, J. Visible-light-induced selective  
34 photocatalytic aerobic oxidation of amines into imines on TiO<sub>2</sub>. *Chem.-Eur. J.* **2012**, *18*, 2624-  
35 2631.  
36

37  
38 (41) Zhang, N.; Li, X.; Ye, H.; Chen, S.; Ju, H.; Liu, D.; Lin, Y.; Ye, W.; Wang, C.; Xu, Q.;  
39 Zhu, J.; Song, L.; Jiang, J.; Xiong, Y. Oxide defect engineering enables to couple solar energy  
40 into oxygen activation. *J. Am. Chem. Soc.* **2016**, *138*, 8928-8935.  
41

42  
43 (42) Su, F.; Mathew, S. C.; Moehlmann, L.; Antonietti, M.; Wang, X.; Blechert, S. Aerobic  
44 oxidative coupling of amines by carbon nitride photocatalysis with visible light. *Angew. Chem.*  
45 *Int. Ed.* **2011**, *50*, 657-660.  
46

47  
48 (43) Huang, Y.; Liu, C.; Li, M.; Li, H.; Li, Y.; Su, R.; Zhang, B. Photoimmobilized Ni clusters  
49 boost photodehydrogenative coupling of amines to imines via enhanced hydrogen evolution  
50 kinetics. *ACS Catal.* **2020**, *10*, 3904-3910.  
51  
52  
53  
54  
55  
56  
57  
58  
59  
60

1  
2  
3 (44) Lang, X.; Ji, H.; Chen, C.; Ma, W.; Zhao, J. Selective formation of imines by aerobic  
4 photocatalytic oxidation of amines on TiO<sub>2</sub>. *Angew. Chem. Int. Ed.* **2011**, *50*, 3934-3937.

5  
6  
7 (45) Xiao, Y.; Tian, G.; Li, W.; Xie, Y.; Jiang, B.; Tian, C.; Zhao, D.; Fu, H. Molecule self-  
8 assembly synthesis of porous few-layer carbon nitride for highly efficient photoredox catalysis.  
9 *J. Am. Chem. Soc.* **2019**, *141*, 2508-2515.  
10  
11  
12  
13  
14  
15  
16  
17  
18  
19  
20  
21  
22  
23  
24  
25  
26  
27  
28  
29  
30  
31  
32  
33  
34  
35  
36  
37  
38  
39  
40  
41  
42  
43  
44  
45  
46  
47  
48  
49  
50  
51  
52  
53  
54  
55  
56  
57  
58  
59  
60